PAPER

Enhanced carrier transport in tris(8-hydroxyquinolinate) aluminum by titanyl phthalocyanine doping

M. Ramar, Priyanka Tyagi, C. K. Suman* and Ritu Srivastava

The effect of doping titanyl phthalocyanine (TiOPc) into tris(8-hydroxyquinolinate) aluminum (Alq$_3$) (Alq$_3$:T; where T represents TiOPc), used as an electron transport layer (ETL) for organic light emitting diodes (OLEDs), was investigated. The surface roughness of the doped thin films increases with the doping concentration as a result of a needle like 3D growth of TiOPc in Alq$_3$. The electron mobility depends on the doping concentration. The electron mobility calculated in the trap-free space-charge limited region (SCLC) for a 2% doped Alq$_3$ thin film was found to be 0.17×10^{-5} cm^2 V^{-1} s^{-1} which is four orders of magnitude greater than that for pristine Alq$_3$. The electroluminescence at a constant current density of 10 mA cm^{-2} is 3098, 4700, 7800, 3600 and 520 cd m^{-2} for Alq$_3$ to Alq$_3$:T(1%, 2%, 3% and 5%) devices, respectively. Similarly the power efficiency at a constant current density of 10 mA cm^{-2} is 2.1, 2.7, 4.2, 1.3 and 0.48 lm W^{-1} for the different doped devices Alq$_3$ to Alq$_3$:T(1%, 2%, 3% and 5%), respectively. The OLEDs based on the optimized 2% doped TiOPc in Alq$_3$ show a four times increase in the electroluminescence as well as an almost doubling of the power efficiency. There are interfacial charges near the doped layer. The Cole–Cole plot indicates the device can be modeled as the combination of three parallel resistance–capacitance (R–C) equivalent circuits.

Introduction

Since the first successful demonstration of organic light emitting diodes (OLEDs) by Tang and Van Slyke,[1,2] good steady progress has been made in improving these devices for use in practical applications. The power consumption and reliability of OLEDs have been key issues for real applications, and remarkable progress has been made through intensive research in the past decade.[3–5] Functional devices based on conjugated polymers or small molecules such as light emitting diodes (OLEDs), organic solar cells (OSCs) and organic field-effect transistors (OFETs) have great potential for light weight, flexible and low-cost electronic and optoelectronic applications.[6] To obtain highly efficient and low-voltage OLEDs, the optimization of charge injection and carrier transport is critically important towards the improvement of device performances.[7,8] The doping of organic semiconductors was first studied in the year 1960,[9] however they have been extensively studied after their use in enhancing the charge carrier injection and transport properties in optoelectronic devices,[10–15] such as OLEDs and OSCs. Despite the extensive studies on p-type and n-type doping of organic semiconductors, doping optimization in organic semiconductors still remains a challenge.

In all of these organic devices, the optimization of the charge injection/extraction and carrier transport is critically important towards their technological success.[16–18] Efficient injection or extraction requires low energetic barriers, while competent transport demands highly conductive transport layers. Organic semiconductors have low carrier concentrations and low carrier mobilities.[18,19] A widely used method for improving electron injection and transport is to employ low-work-function metals, either as individual layers in contact with the cathode or as n-type conductive dopants in the organic electron-injection layers (EILs), which can help to reduce the injection barrier at the electrode/organic interface and provide excellent electron injection from the cathode to the organic layer.[20–24] Alkali metals such as Li, Cs and their oxides have also been used for n-type conductive doping of organic electron transport materials[25–27] and were found to be useful in many instances. However, this type of doping has lots of problems, including damage to the underlying organic layers due to the tendency to diffuse in the organic materials. For this reason, there is a need for molecular dopants to enhance the electron transporting properties and for use in OLED applications.

Here, we have compared the use of TiOPc as an n-type dopant of Alq$_3$ at different concentrations. The thin films of doped and undoped materials were studied and investigated for their application in lighting devices (OLEDs).

CSIR-Network of Institutes for Solar Energy, Physics of Energy Harvesting division, CSIR-National Physical Laboratory, New Delhi, India. E-mail: cksuman@gmail.com

Experimental methods

The electron only devices were fabricated with the structure $Al|Alq_3:TiOPc|Al$. The Alq_3 was doped with TiOPc with weight percentage doping concentrations of 1, 2, 3 and 5%; those thin films and devices were named as $Alq_3:T1$, $Alq_3:T2$, $Alq_3:T3$ and $Alq_3:T5$, respectively. The doping of the organic layers was performed by a thermal co-evaporation process. Similarly, light emitting diodes (OLEDs) were fabricated on indium-tin-oxide (ITO) (purchased from Vin Karola USA) coated glass substrates with a sheet resistance of 20 Ω sq^{-1}. Before depositing all organic materials, the ITO substrates were cleaned ultrasonically with de-ionized water, acetone and isopropyl alcohol, and finally dried. The deposition rate was kept at 1–2 Å s^{-1} for the organic layers and 2–5 Å s^{-1} for the aluminum as the metal cathode. The overlap of the ITO anode and the Al cathode defines the active area of the device to be 6 mm^2.

The current density–voltage (J–V), current density–voltage–luminescence (J–V–L) and current efficiency–current density–power efficiency characteristics of the OLEDs were measured simultaneously with a programmable Keithley 2400 power source and a Luminance meter (LMT-1009). Impedance spectroscopy (IS) measurements were performed using an Impedance/Gain-Phase Analyzer (Solartron, model SI 1260) Characterization System. A 100 mV amplitude AC signal superimposed on a DC bias was used to measure the device impedance as a function of the AC frequency and DC bias.

Results and discussion

The surface morphologies of the doped and undoped Alq_3 thin films were characterized by atomic force microscopy (AFM). Fig. 1(A)–(E) show the AFM images of Alq_3, $Alq_3:T1$, $Alq_3:T2$, $Alq_3:T3$ and $Alq_3:T5$. The surface roughness increases with increasing the concentration of TiOPc. The RMS values of roughness are 0.3914 nm, 0.5549 nm, 0.5742 nm, 0.6146 nm and 6.2326 nm for Alq_3, $Alq_3:T1$, $Alq_3:T2$, $Alq_3:T3$ and $Alq_3:T5$ respectively. The thin films of Alq_3, $Alq_3:T1$ and $Alq_3:T2$ consist of small uniform 3D islands with a compact shape. The surface morphology changes drastically if the doping concentration is increased above 2%: an island shape transition occurs resulting in typical needle-like structures with elongated 3D-islands. Fig. 1(E) shows that the islands become thereby progressively longer, quickly reaching a fixed asymptotic width while their height remains much longer than their width. Hence high doping concentrations of TiOPc are not suitable for device application.

Since the Al work function is about 4.2 eV and the Alq_3 LUMO value is 3.0 eV,[28] the electron injection barrier between Al and Alq_3 will be very high. However, in between the Al and Alq_3 films it is observed that there are large interface dipoles present,[29] which reduces the electron injection barrier by about 1.0 eV, hence the net barrier present is 0.2 eV. In the same way, the energy barrier for hole injection is increased by 1.0 eV due to the interface dipole and the resultant barrier for hole injection becomes 2.5 eV. Therefore, holes are not injected compared to the injection of electrons, and any current observed in the
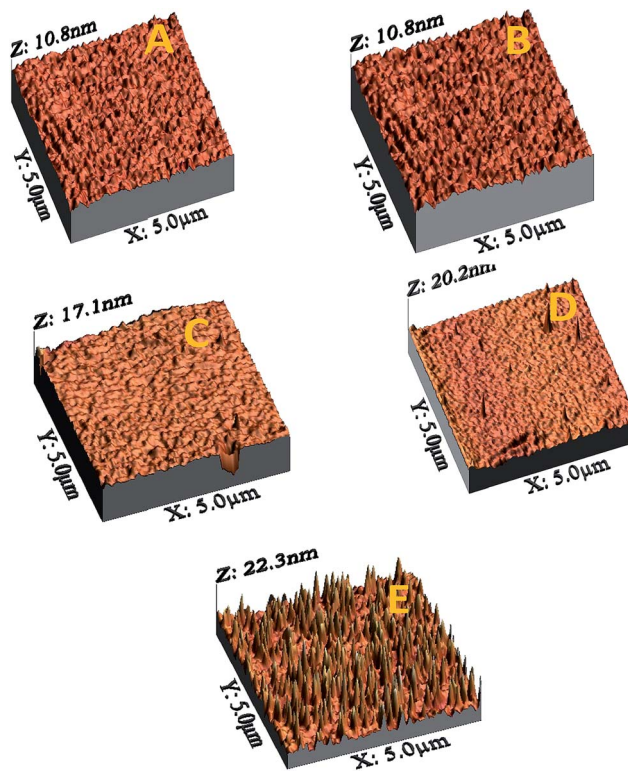

Fig. 1 The AFM images (5 μm × 5 μm) of TiOPc doped Alq_3 thin films; (A) Alq_3, (B) $Alq_3:T1$, (C) $Alq_3:T2$, (D) $Alq_3:T3$ and (E) $Alq_3:T5$.

device will be only due to electrons flowing between the two Al electrodes. Therefore, the electron only devices can be considered to have the structure of Al/organic/Al. The thicknesses of the organic films were kept at 100 nm for all of the five devices. Fig. 2 shows the J–V characteristics of the electron only Alq_3, $Alq_3:T1$, $Alq_3:T2$, $Alq_3:T3$ and $Alq_3:T5$ devices. The inset of Fig. 2 shows an enlarged J–V plot with a logarithmic x axis. It is clearly shown in the inset figure that the driving voltage of the electron
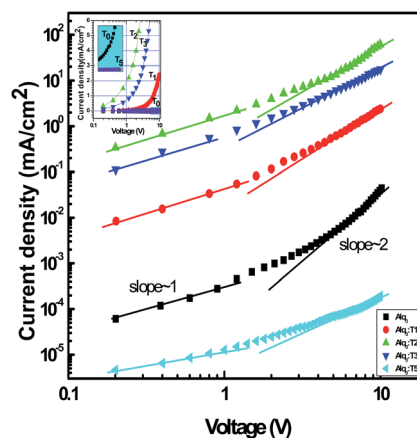

Fig. 2 The current density–voltage (J–V) characteristics of the electron only devices of the $Alq_3:TiOPc$ thin films. The structure of the device was $Al/Alq_3:T$ (1–5%)/Al. Inset: an enlarged view of the J–V characteristics with a logarithmic x axis.

only devices shifts with the doping concentration. The current density increases linearly with the increase of voltage in the lower voltage region, and in the high voltage region the current density increases non-linearly for all of the devices. At low voltages (the first region of the J–V curve), the slope of the log J–V plots are approximately unity, while at higher voltages, the slope is about 2 or more. Hence the conductivity is clearly Ohmic at low voltage and exhibits space charge limited conductivity (SCLC) at higher voltages. In the Ohmic region of the conductivity, the current density can be expressed as $J = q n_0 \mu \dfrac{v}{d}$, where n_0 is the concentration of thermally activated carriers, μ is the mobility and d is the thickness of the organic semiconductor used ($d = 100$ nm). In the high voltage region (the second region of the J–V curve) $J \propto V^2$ indicating a limited current controlled by a space charge with a single discrete set of shallow traps. The current density in this region is $J = \dfrac{9}{8} \varepsilon \mu \theta \dfrac{v^2}{d^3}$, where ε is the organic semiconductor dielectric constant (taken as 3.5), μ is the charge carrier mobility and θ is the trapping fraction. The trapping fraction can be represented by $\theta = \dfrac{n_0}{n_0 + n_t}$, where n_0 is the free charge carrier density and n_t is the trapped charge carrier density. The electron mobility of Alq$_3$, calculated assuming trap free SCLC ($n_t = 0$), was 0.62×10^{-8} cm^2 V^{-1} s^{-1} which is comparable to the mobility obtained from the TOF technique.[30] The mobilities for the doped thin films are 0.7×10^{-7}, 0.17×10^{-5}, 0.75×10^{-6} and 0.68×10^{-9} cm^2 V^{-1} s^{-1} for Alq$_3$:T1, Alq$_3$:T2, Alq$_3$:T3 and Alq$_3$:T5, respectively. The mobility for the Alq$_3$:T2 thin film is higher than all of the four other dopant concentrations in the thin films. The electron mobility of the Alq$_3$:T2 thin film is four orders of magnitude greater than that of the Alq$_3$ device. The suitable doping concentration provides new hopping sites for the carrier that leads to an increased mobility in the organic semiconductor. The other reasons for the enhanced electron mobility may be the broadening of the density of states and charge transfer.[31] Doping Alq$_3$ with common inorganic insulators (Li salts) creates radical ions of Alq$_3$ which are responsible for the n type doping effect. Similar negative charge enriched thin films are achieved by organic molecular doping.[32]

Fig. 3 shows (A) the energy level diagram of the OLED and (B) the electroluminescence spectra of the device at different bias voltages. The inset of Fig. 3(B) shows photographs of the light output at bias voltages of 8 V and 15 V. The fabricated OLED structure consists of 35 nm N,N'-di(naphthalene-1-yl)-N,N'-diphenylbenzidine (NPB) as a hole-transporting layer (HTL), 35 nm tris(2-phenylpyridine)iridium(III) [Ir(ppy)$_3$] (5%) doped in a 4,4′-bis-(carbazol-9-yl)-biphenyl (CBP) green light emitting layer (EML), a 6 nm-thick 2,9-dimethyl-4,7-diphenyl-1,10-phenanthroline (BCP) hole-blocking layer (HBL) and a 28 nm thick titanyl phthalocyanine (TiOPc) doped tris(8-hydroxyquinolinato) aluminum (Alq$_3$) electron transport layer (ETL). The doping of Ir(ppy)$_3$ into the CBP facilitated the control of triplet quenching at the interfaces. ITO and lithium fluoride (LiF) (1 nm)/aluminium (Al) (100 nm) were used for the anode and cathode, respectively. The device structure of the green
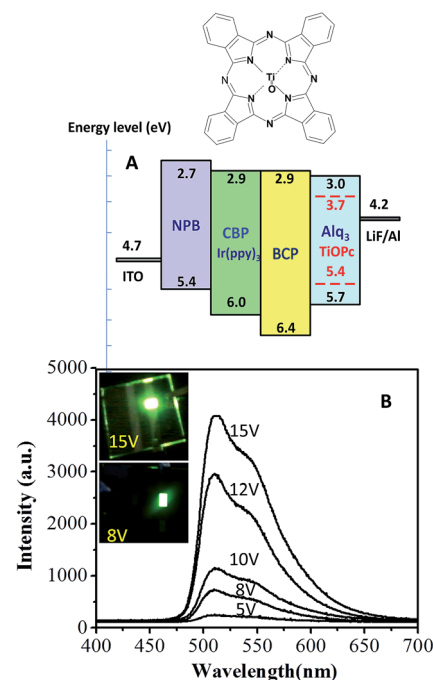

Fig. 3 (A) The molecular structure of TiOPc and an energy level diagram for the OLEDs. (B) The electroluminescence spectra of the OLEDs at different bias voltages; the inset shows photographs of the light output at 8 V and 15 V bias voltages.

phosphorescent OLEDs is [ITO/NPB/CBP:Ir(ppy)$_3$/BCP/Alq$_3$:T(x)/LiF/Al]. The EL spectra showed an emission only from Ir(ppy)$_3$ with no emission from the neighboring materials. The emission pattern is in the green spectral range of the visible regime, with its main peaks at 515 nm and an additional shoulder at 550 nm. There is no significant shift in the position of the emission peaks within the applied bias range. The emission color is stable in the investigated bias voltage region.

Fig. 4 shows the J–V–L characteristics of the OLEDs containing Alq$_3$, Alq$_3$:T1, Alq$_3$:T2, Alq$_3$:T3 and Alq$_3$:T5 as the ETLs,
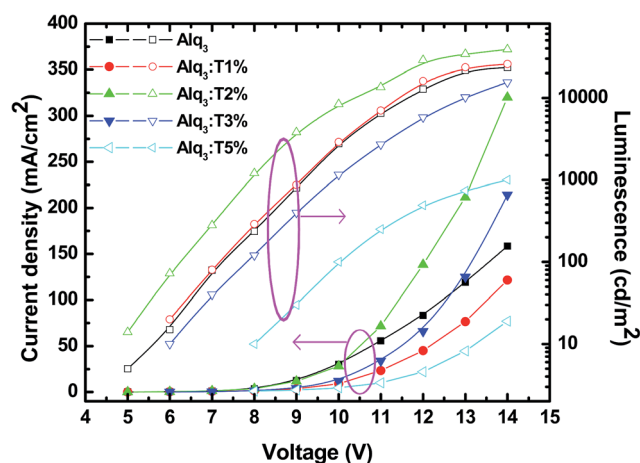

Fig. 4 The current density–voltage–luminescence (J–V–L) characteristics of devices with different doping quantities of TiOPc with Alq$_3$.

respectively. The current density at high voltage increases with the TiOPc doping concentration up to 2%. Above 2% doping the value of the current density is found to be low in comparison to undoped ETL. At a fixed bias of 11 V, the current density of the devices containing Alq_3, Alq_3:T1, Alq_3:T2, Alq_3:T3 and Alq_3:T5 are 57.81, 24.35, 72.35, 47.62 and 11.26 mA cm^{-2}, respectively. The current density of the Alq_3:T2 OLED increased by 25% compared to the pristine Alq_3 device. The driving voltage is reduced for the T2 device, which indicates the enhancement of the electron injection and transport by suitable ETLs. The luminescences of the devices based on Alq_3 to Alq_3:T5 at a current density of 10 mA cm^{-2} are 3098, 4700, 7800, 3600 and 520 cd m^{-2}, respectively. At this value of current density, the luminescence is doubled. This enhancement in electroluminescence may be attributed to the enhancement of the holes and electrons recombination rate.

Fig. 5(a) and (b) show the current efficiency and power efficiency as a function of current density for the Alq_3 to Alq_3:T5 devices, respectively. It can be clearly observed in Fig. 5(a) and (b) that the trend in the efficiencies is consistent with the variation of the electrical properties of the devices with the use of different ETLs, and the improved electrical properties lead to the enhanced device efficiency. These results indicate that the TiOPc doping provides a balance of carriers. The control of both carriers in the device gives high yield electroluminescence. At a 35.19 mA cm^{-2} current density, the current efficiency of Alq_3:T2 is five times that of the Alq_3 devices. At a current density of 10 mA cm^{-2}, the power efficiency of the Alq_3:T2 device doubled compared to the pristine Alq_3 device. The overall current efficiency and power efficiency was increased for the 2% doped devices.

The capacitance–voltage (C–V) studies provide information on the electronic properties of the OLEDs. The C–V characteristics were measured at a fixed frequency of 1000 Hz under dark conditions as shown in Fig. 6. At negative to positive bias (−2 to 4 V), a constant capacitance was observed that corresponds to the geometrical capacitance of the device. The capacitances of all of the devices start increasing with the increase of bias voltage (above 4 V) and after reaching maximum values, they start to decrease for further increases of bias
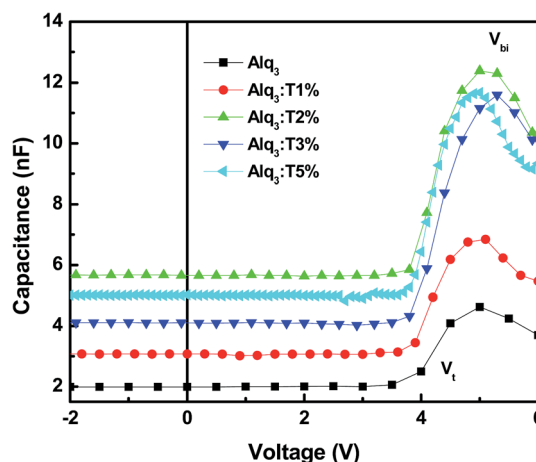

Fig. 6 Capacitance–voltage (C–V) characteristics of the OLEDs at a frequency of 1000 Hz.

voltage. The increase of capacitance may be due to the accumulation of charge at the Alq_3:TiOPc interface. As the electrons and holes recombined, the charge is annihilated, thus the capacitance decreases rapidly with the increasing of applied bias. Since, $V_t \neq V_{bi}$ it simply means that a negative interfacial charge density σ_{if} is present. Its value can be calculated from the following equation:[33,34]

$$\sigma_{if} = Q_{if}/A = \frac{\varepsilon_0 \varepsilon_r}{d_{Alq_3:T}}(V_t - V_{bi}) \tag{1}$$

with $\varepsilon_r \approx 3$, $A = 6$ mm^2 and $d_{Alq_3} = 30$ nm. The Q_{if} and σ_{if} for all of the studied devices Alq_3 to Alq_3:T5 are −2.95, −2.9, −4.6, −4.2, and −2.5 nC and −0.49, −0.48, −0.77, −0.7 and −0.42 mC m^{-2}, respectively. In the case of no interfacial charge the threshold voltage and the built-in voltage would be equal ($V_t = V_{bi}$), as the flat-band case would be reached simultaneously in the TiOPc and the Alq_3 layer.

The Cole–Cole plots of all of the devices at a 0 V bias and room temperature are shown in Fig. 7. The equivalent circuit of these devices consists of a parallel resistance (R_P) and capacitance (C_P) network in series with the contact resistance (R_S). The
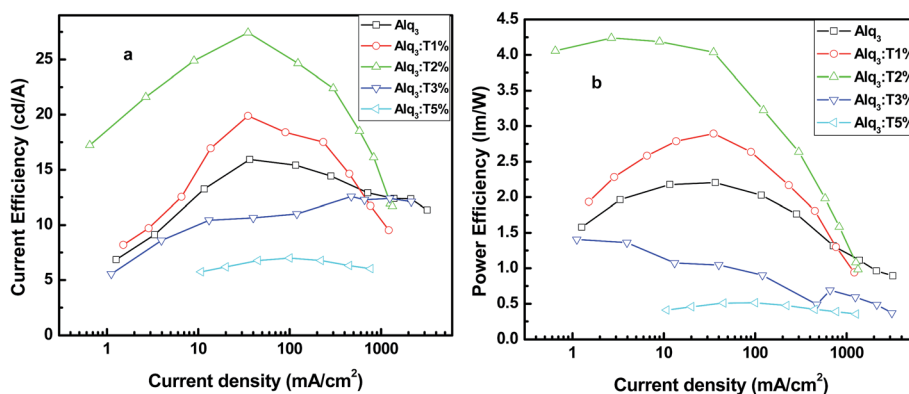

Fig. 5 (a) Current efficiency vs. current density characteristics of the Alq_3 and Alq_3:T(1, 2, 3 & 5%) devices; (b) power efficiency–current density characteristics of the Alq_3 and Alq_3:T(1, 2, 3 & 5%) devices.
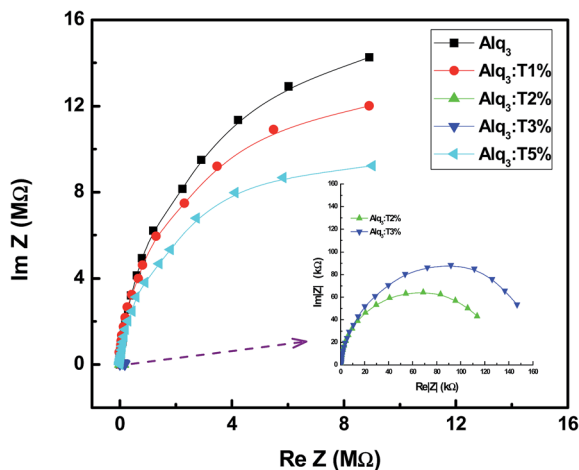
Fig. 7 Cole–Cole plot of the Alq$_3$ and Alq$_3$:T(1, 2,3 &5%) OLEDs at a 0 V bias. The inset shows an enlarged curve for the Alq$_3$:T2 and Alq$_3$:T3 devices.

R_S circuit element that corresponds to the intersection of the semicircle at high frequencies represents resistive losses at the ITO and Al electrodes. In this work, we have shown the equivalent R–C electrical circuit for a three layered structure of a device in which NPB is the hole transporting layer, CBP:Ir(ppy)$_3$ is the emissive layer and Alq$_3$:T is the electron transport layer, which consists of three parallel R–C circuits connected in series with contact resistance ($R_S \sim 0\ \Omega$) as shown in the inset of Fig. 7. From Fig. 7, it is observed that the diameter of the semicircle is highly dependent on the resistance of the devices, which represents the bulk resistance of the organic layers R_{b1} to R_{b3}. The decrease in the diameter of the semicircle is in response to the increase of the resistance of the TiOPc doped Alq$_3$ layer which is also reflected in the J–V characteristics (Fig. 4). The equivalent resistance for devices Alq$_3$ to Alq$_3$:T5 are 10 MΩ, 8 MΩ, 70 kΩ, 90 kΩ and 6 MΩ, respectively.

Conclusion

In conclusion, the doping of TiOPc into Alq$_3$ contributes to an increase of the electron mobility in the Alq$_3$, and as a result the performance of the related OLEDs are enhanced. The increase in mobility is attributed to the addition of new hopping sites for carriers after doping. The surface roughness increases with doping concentrations, and the optimized roughness is found to be 0.5742 nm for 2% doping. The electron transport is well described by space-charge limited current in the doped and pristine studied thin films of Alq$_3$. The electron mobility of the 2% doped thin films is 0.17×10^{-5} cm^2 V^{-1} s^{-1} which is three orders of magnitude greater than that of the Alq$_3$ film. The electroluminescence ($\sim$7800 cd m^{-2}) at a current density of 10 mA cm^{-2} is 2.6 times higher than that of the undoped device. The interfacial charge density for the 2% doped OLED device is -0.77 mC m^{-2}. The Cole–Cole plot of the OLEDs can be modeled as the combination of three parallel resistance–capacitance (R–C) equivalent circuits with a series resistance ($R_S \sim 0\ \Omega$). The equivalent resistance of the optimized device (2% doping) is 70 kΩ whereas the resistances of the other devices are in the mega-ohm range.

References

1 C. W. Tang and V. Slyke, *Appl. Phys. Lett.*, 1987, **51**, 913.
2 C. W. Tang, V. Slyke and C. H. Chen, *J. Appl. Phys.*, 1989, **65**, 3610.
3 M. A. Baldo, D. F. O′ Brien, Y. You, *et al.*, *Nature*, 1998, **395**, 151.
4 V. E. Choong, S. Shi, J. Curless, *et al.*, *Appl. Phys. Lett.*, 1999, **75**, 172.
5 S. A. V. Slyke, C. H. Chen and C. W. Tang, *Appl. Phys. Lett.*, 1996, **69**, 2160.
6 R. Steyrleuthner, S. Bange and D. Nehar, *J. Appl. Phys.*, 2009, **105**, 064509.
7 L. S. Hung, C. W. Tang and M. G. Mason, *Appl. Phys. Lett.*, 1997, **70**, 152.
8 Z. Xu, L. M. Chen, G. Yang, C. H. Huang, J. Hou, Y. Wu, G. Li, C. S. Hsu and Y. Yang, *Adv. Funct. Mater.*, 2009, **19**, 1227.
9 M. Pope and C. E. Swenberg, *Electronic Process in Organic Crystals and Polymers*, Oxford University Press, Oxford, U.K, 1999.
10 M. Pfeiffer, A. Beyer, T. Fritz and K. Leo, *Appl. Phys. Lett.*, 1998, **73**, 729.
11 M. Pfeiffer, A. Beyer, T. Fritz and K. Leo, *Appl. Phys. Lett.*, 1998, **73**, 3202.
12 M. Pfeiffer, T. Fritz, J. Blochwitz, A. Nollau, B. Plonnigs, A. Beyer and K. Leo, *Adv. Solid State Phys.*, 1999, **39**, 77.
13 C. Ganzorig and M. Fujihira, *Appl. Phys. Lett.*, 2000, **77**, 4211.
14 X. Zhou, M. Pfeiffer, J. Blochwitz, A. Werner, A. Nollau, T. Fritz and K. Leo, *Appl. Phys. Lett.*, 2001, **78**, 410.
15 A. Kumar, R. Srivastava, P. Tyagi and D. S. Mehta, *J. Appl. Phys. Lett.*, 2011, **109**, 114511.
16 K. R. Choudhury, J. H. Yoon and F. So, *Adv. Mater.*, 2008, **20**, 1456.
17 Y. Shirota and H. Kageyama, *Chem. Rev.*, 2007, **107**, 953.
18 V. Coropceanu, J. Comil, D. A. S. Filho, Y. Oliver, Y. Silve and J. L. Bredas, *Chem. Rev.*, 2007, **107**, 926.
19 W. Brutting, S. Berleb and A. G. Muckl, *Org. Electron.*, 2001, **2**, 1.
20 K. Walzer, B. Maening, M. M. Pfeiffer and K. Leo, *Chem. Rev.*, 2007, **107**, 1233.
21 W. Ou-yang, M. Weis, X. Chen, T. Manaka and M. Iwamoto, *J. Chem. Phys.*, 2009, **131**, 104702.
22 Y. Zhou, C. Fuentes-Hernandez, J. Shim, J. Meyer, A. J. Giodano, H. Li, P. Winget, T. Papadopoulos, H. Cheun, J. Kim, M. Fenoll, A. Dindar, W. Haske, E. Najafabadi, T. M. Khan, H. Sojoudi, S. Barlow, S. Graham, J. L. Bredas, S. R. Marder, A. Khan and B. Kippelen, *Science*, 2012, **336**, 327.

23 D. Taguchi, T. Shino, X. Chen, L. Zhang, J. Li, M. Weis, T. Manaka and M. iwamoto, *J. Appl. Phys.*, 2011, **110**, 103717.

24 Y. H. Deng, Y. Q. Li, Q. D. Ou, Q. K. Wang, F. Z. Sun, X. Y. Chen and J. X. Tang, *Org. Electron.*, 2014, **15**, 1215.

25 J. Kido, K. Nagai and Y. Okamoto, *IEEE Trans. Electron Devices*, 1993, **40**, 1342.

26 J. Kido and T. Matsumoto, *Appl. Phys. Lett.*, 1998, **73**, 2866.

27 A. Werner, F. Li, K. Harada, M. Pfeiffer, T. Fritz, K. Leo and S. Machill, *Adv. Funct. Mater.*, 2004, **14**, 255.

28 R. Q. Zhang, C. S. Lee and S. T. Lee, *J. Chem. Phys.*, 2000, **112**, 8614.

29 H. Ishii, K. Sugiyama, E. Ito and K. Seki, *Adv. Mater.*, 1999, **11**, 605.

30 G. G. Malliaras, Y. Sen, D. H. Dunlup, H. Murata and Z. H. Kafafi, *Appl. Phys. Lett.*, 2001, **79**, 2582.

31 O. Tal, Y. Rosenwaks, Y. Preezant, N. Tessler, C. K. Chan III and A. Kahn, *Phys. Rev. Lett.*, 2005, **95**, 256405.

32 P.-C. Kao, J.-H. Lin, J.-Y. Wang, C.-H. Yang and S.-H. Chen, *J. Appl. Phys.*, 2011, **109**, 094505.

33 W. Brutting, S. Berleb and A. G. Muckl, *Org. Electron.*, 2001, **2**, 1.

34 S. Nowy, W. Ren, J. Wagner, J. A. Weber and W. Brutting, *Proc. SPIE*, 2009, **7415**, 74150G-1.